

A New Optimal Correlation for Behavior factor of EBFs under Near-fault Earthquakes using Artificial Intelligence Models

Seyed Abdonnabi Razavi ¹; Navid Siahpolo ²

Abstract

Abstract:


Behavior factor of the structures is a coefficient that includes the inelastic performance of the structure and indicates the hidden resistance of the structure in the inelastic stage. In most seismic codes, this coefficient is merely dependent on the type of lateral resistance system and is introduced with a fixed number. However, there is a relationship between the behavior factor, ductility (performance level), structural geometric properties, and type of earthquake (near and far). In this paper, a new optimal correlation is attempted to predict the behavior factor (q) of EBF steel frames, under near-fault earthquakes, using *Particle Swarm Optimization (PSO)* and *Simulated Annealing (SA)* algorithms. For this purpose, a databank consists of 12960 data created. To establishing different geometrical properties of models, 3-, 6-, 9-, 12-, 15, 20- stories steel EBF frames considered with 3 different types of link beam, 3 different types of column stiffness and 3 different types of brace slenderness. Using nonlinear time history under 20 near-fault earthquake, all models analyzed to reach 4 different performance level. data were used as training data of the *Artificial Intelligence Models*. Results shows the high accuracy of proposed correlation, established by PSO algorithm. The results of the correlation between the studied algorithms show more accuracy in the relations produced than the previous algorithms and confirm the significance of the governing relations.

Keywords: Artificial Intelligence Models; Particle Swarm Optimization (PSO); Simulated Annealing (SA); Behavior factor; Performance levels.

Introduction

The experience of earlier earthquakes confirms that, the structural responses enters to the nonlinear area, depending on the severity and content of the earthquake. Evaluation of the nonlinear responses, shows that the base shear force demands are reduced in this case. The reduction in the reaction force and its conversion to the in-elastic base shear force is defined in many seismic codes with a behavior factor (resistance reduction coefficient). These coefficients are generally obtained from

empirical studies. The task of these coefficients is to consider all the nonlinear effects of the structure [1]. The major drawback to these coefficients is that it is assumed to be constant for structures with different performance levels and cannot provide a good picture of the nonlinearity levels of the structure and its components. For example, if the behavior factor of the structure is lower than its actual value, the forces applied to it are more likely to be considered and can lead to non-economic design. Conversely, if the chosen behavior factor is greater than its actual value, the base shear force

 Corresponding author: Razavi@iauabadan.ac.ir

1. 1Department of Civil Engineering, Abadan branch, Islamic Azad University, Abadan, Iran
2. 2Department of Civil Engineering, Institute for Higher Education ACECR, Khuzestan, Iran

is less than the real value. In this case, it seems that, as the structure enters to the in-elastic region, the deformation demands of the members become greater than the structure strength, thereafter damage to the structure occurs. Recent research shows that seismic demands on beams and braces are highly related to overstrength of links at corresponding story [2]. Also, higher modes of EBF play an important role in the seismic response of high-rise EBF, and seismic axial force demand on columns is less than that recommended in codes [3].

Gerami *et al.* (2014) showed that the structural responses of eccentrically braced frame (EBF) structures is very sensitive to the acceleration pulse continuity due to the near-fault records [4]. Other observations showed that the main response of structures due to near-fault earthquake with fling-step effects (permanent displacement at strike-parallel direction of a strike-slip fault) was obtained at the first mode of the structures [5, 6]. Gerami *et al.* (2013), studied steel moment resisting frames under near fault earthquakes with pulse velocities greater than 0.70s and showed that the effects of forward directivity increased the global and local demands about 1.1–2.6 and 1.2–3.5 times, respectively [7]. Also, Mashayekhi *et al.* (2019) illustrate that the inter-story drift angle of structures under near fault earthquakes with forward directivity effect is greater than far fault earthquakes for about 30–50% of structure height in upper stories [8].

Recently, the use of artificial intelligence models, has been welcomed by many researchers in optimizing the relationships governing the design of steel structures [9, 10]. A heuristic particle swarm optimizer (HPSO) algorithm, developed by Li *et al.* (2009) [11] for truss structures with discrete variables which has all the advantages that belong to the convenient algorithms, and has faster convergence rate than the particle swarm optimization (PSO) and particle swarm optimization with passive congregation (PSOPC) for discrete variables. The particle swarm optimizer is used to develop an optimum design algorithm for moment resisting steel frame by Dogan *et al.* (2012) [12]. They used the optimum design algorithm to select the optimum W-sections from American steel sections table for beams and columns of unbraced frame such that design constraints

described in the code "LRFD–AISC" are satisfied and the frame has the minimum weight. Chatterjee *et al.* (2017) employed the PSO to find a weight vector with minimum root-mean-square error (RMSE) for detecting the failure possibility of the multistoried RC building structure, using a database of 150 multistoried buildings' RC structures [13]. Lamberti (2008) presents a Simulated Annealing-based algorithm denoted as CMLPSA⁴. CMLPSA is tested in six structural optimization problems where the objective is to minimize the weight of bar trusses – with up to 200 elements – subject to constraints on nodal displacements, member stresses and critical buckling loads [14]. Development of hybrid optimization algorithm for structures furnished with seismic damper devices using the particle swarm optimization method and gravitational search algorithm was done by Ayyash *et al.* (2022) [15]. A two-phase SA approach was proposed for acquiring optimum design of steel lattice towers with an annealing algorithm by Tort *et al.* (2017) [16]. In the first phase of this method, only the layout parameters are optimized by annealing algorithm while the steel members are sized with a fully stressed design based heuristic approach. In the second phase, the best design obtained in the prior phase is utilized as the initial design, and the annealing algorithm is implemented anew for both layout and size variables together under a new set of annealing parameters over a much reduced number of cooling cycles [16]. The modified simulated annealing algorithm (MSAA) is employed to solve optimal design of steel structures by Millan *et al.* (2019) [17].

This article proposes an optimal simple expression for estimating of behavior factor of the EBFs. These formulae are expressed based on geometrical characteristics of EBFs and are obtained based on parametric study including numerous nonlinear time history analyses of 162 EBFs with 4 performance levels under 20 near-fault ground motions. The considered geometrical characteristics include the number of stories, the brace slenderness, and the stiffness of the columns and the ratio of the link beam length to the total length of the beam. For this purpose, it is necessary to prepare a large database of studies of a considerable number of frames with an eccentrically braced frame system, using nonlinear dynamic analysis. A

4 . Corrected Multi-Level & Multi-Point Simulated Annealing

total of 12960 nonlinear analyzes were performed on the basis of a platform of IDA⁵ analysis to create a database containing a wide range of relevant data. For this purpose, two optimization algorithms are used to estimate the behavior factor, and at the end, the optimal relationship is presented as the research result. It can be perceived that outcomes of the proposed patterns are in good agreement with the exact results of nonlinear time history analyses. The main emphasis is on introducing of the potential of the proposed relationships to fit them into the framework of design methods based on elastic analysis. In this process, for a given behavior factor, q , the presented relationships can provide the designer with an acceptable estimate of the maximum roof displacement, the maximum inter-story drift, and other structural demands.

Although much research work has been carried out to propose more applicative R - μ relationships, the results are mainly focused on structures under far-field earthquakes, which this study is under near-field motions. It has been recognized by researchers that seismic ground motions close to an active fault could be extremely different than far-field (FF) ground motion records and could demonstrate unusual spectral shape, as well as large amplitude and different energy content. In near-fault (NF) zones, due to the short distance between the rupture fault and building site, high-frequency damping is minimal and so their records include high-frequency contents. By far, no results are available regarding the R - μ relationships for structures subjected to severe Near-fault pulse-like (NF-PL) ground motions. Generally, the structural responses due to NF-PL are coupled with those induced by FF, making it complicated to build reasonable responses. Another highlight of the present study is prediction a correlation based on artificial intelligence models which has more accuracy in compare with correlations established based on a simple regression. The use of optimization algorithms when there is a large amount of data seems to be very important to increase the accuracy of production relationships. Meanwhile, another highlight of the proposed intelligent model is being depend on the different levels of performance. Therefore, it can reduce complex complications while receiving more accurate responses by

establishing a connection between elastic and non-elastic design.

2. PSO Algorithm

PSO is a metaheuristic optimization algorithm that is modeled on the base of movements of a group of birds or groups of fish that live in groups. This algorithm uses the concept of social interaction to solve the problems. The relationships between particle swarm optimization described by Kennedy *et al.* in (1995) [18] for the first time, and modified by Shi *et al.* in (1998) [19]. This algorithm, was first used to solve the problems of electrical engineering, electronics and telecommunications. PSO, shows the optimal movement of flying birds for accurate detection and takes the optimal shape by analyzing flight patterns. Studies show that the change in the direction of each particle is based on the flight pattern of the neighboring particles, and each particle imitates the other particles. Particle position change is based on experience and its and other particle knowledge's. The result of modeling this social behavior is the process of searching for particles that tend toward a better position. Particles use each other's knowledge to learn, and each particle goes to the best particle according to the knowledge obtained. If, the particle finds a better position than the particle in question, the other particles will align with it. This algorithm, uses a population that includes potential problem-solving solutions that it uses to explore the search space. The main difference between this method and other methods is that each particle has a velocity vector that, by changing it, continuously searches in the decision space. This vector has two components, which include the motion of the particle in the best position it has ever encountered and the best position that the particle has reached in the whole population. It is attracted towards the location of the best fitness achieved so far by the particle itself and by the location of the best fitness achieved so far across the whole population [20].

The process of working in PSO is that in order to achieve the optimal response, the particles are first randomly selected with zero initial velocity. In the next steps, the particles have acceleration and velocity, so that the motion and displacement of each particle and the position of the particle in the new position are calculated according to the previous position and velocity. In the partial

PSO, the speed and position of each particle change according the equality role [19]. The formula for the speed and the position of the particle in the whole PSO is completely identical [21]. After quantification, the next step is to examine the particles in terms of their suitability and value. Then, according to the location of each particle in the group and the best global location, the particles are compared and the best

$$X_{k+1}^d = X_k^d + v_{k+1}^d \quad (1)$$

while the velocity v^d is updated as

$$v_{k+1}^d = v_k^d + c_1 r_1 (p_k^d - x_k^d) + c_2 r_2 (p_k^g - x_k^g) \quad (2)$$

Here, the subscript k indicates a pseudo-time increment. p_k^d represents the best previous position of particle d at time k , while p_k^g represents the global best position in the swarm at time k . r_1 and r_2 represent uniform random numbers between 0 and 1 [19]. Kennedy and Eberhart propose that $c_1 = c_2 = 2$, in order to

$$v_{k+1}^d = \omega v_k^d + c_1 r_1 (p_k^d - x_k^d) + c_2 r_2 (p_k^g - x_k^g) \quad (3)$$

They proposed that w be selected such that $0.8 < w < 1.4$. In addition, they reported improved convergence rates when w is decreased linearly during the optimization [19]. In local PSO, instead of persuading the optimist particle of the swarm, each particle will pursuit the optimist particle in its surrounding to regulate its speed and position [21]. The flowchart of performing PSO is shown in **Figure 1**.

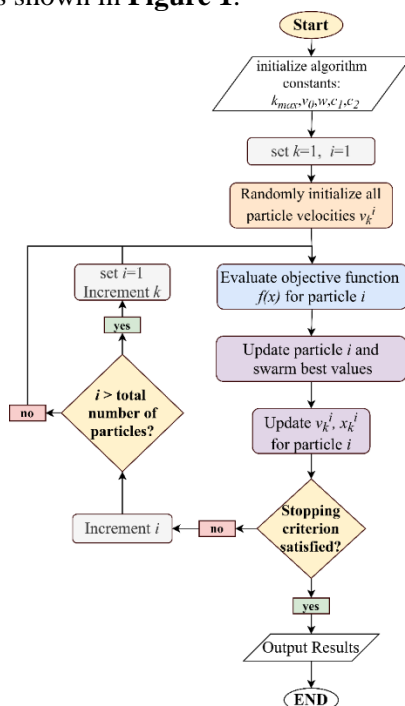


Figure 1: Flowchart of PSO algorithm [23]

value of each particle and the best global value among the group are determined. Then, if the intended goal is achieved, the search for the particles is completed and otherwise the particle is evaluated again to continue the process, the criterion to be examined. Kennedy and Eberhart (1995) [19] originally proposed that the position X^d be updated as :

allow a mean of 1 (when multiplied by the random numbers r_1 and r_2) [19]. The result of using these proposed values is that birds *overfly* the target half the time [22]. Shi and Eberhart (1998) [19] later introduced an inertia term w by modifying **Equation (2)** to become :

3. SA Algorithm

One of the most useful algorithms for solving problems that cannot be managed due to the increasing number of variables, is the Simulated Annealing (SA) algorithm. This algorithm is mainly used to estimate or optimize large space problems. The SA algorithm is essentially an expanded understanding of the concept of the annealing process in metallurgy engineering. Annealing refers to heat treatment in which the physical and sometimes chemical properties of a substance change. During this process, the metal is first heated, then kept at a certain temperature, and finally, gradually cooled. As the metal heats up, the molecules move freely everywhere. With the gradual cooling of the material, this freedom decreases. If the cooling process is slow enough to ensure that the metal is in thermodynamic equilibrium at each stage, it can be ensured that the heat energy is evenly distributed in the body and that it has the best crystal structure that is symmetrical and durable. In the SA algorithm, the process is modeled. The SA algorithm introduced firstly in 1983 by Kirkpatrick *et al.* [24]. The SA algorithm is basically a metaheuristic algorithm. In this algorithm, probabilistic methods are used to solve the optimization problem.

Since its introduction as a generic heuristic for discrete optimization, SA has become a popular tool for tackling both discrete and

continuous problems across a broad range of application areas [25]. In this algorithm, point s is considered a state of the physical system and the function $E(s)$ is similar to the internal energy of the system in s state. Basically, the goal is to start the system from a desired initial state (for example, a desired s_0) to a state (S_n) where the $E(s)$ function is minimal. In fact, starting from a desired state, from the physical system, it reaches a state in which the internal energy of the system is minimal (the system will have the least energy in that state). To do this, the algorithm starts from a desired point and then selects a neighbor mode. After that, it probably decides to stay in the current state or move to the neighboring state. The sum of these possible displacements leads the system to a state with less internal energy. This is done until the system reaches a rational state or the amount of calculations exceeds a certain threshold. The key step of SA is probability calculation, which involves building

the annealing schedule [26]. The probability of transfer from a current state (eg. s) to a new candidate state (such as s') is determined by a function of the probability of accepting $P(e, e', T)$, where $e = E(s)$ and $e' = E(s')$. The E function indicates the internal energy of the system and the T indicates the temperature. The temperature T changes over time. Since the goal of the algorithm is to minimize the energy of the system, the state in which the $E(s)$ is less will be more optimal. This acceptance rule for new states is referred to as the *Metropolis criterion* [27]. The remarkable thing about the SA algorithm is that the probability function of P must always be positive, even if e is smaller than e' . This feature prevents the algorithm from stopping in the "local optimum" mode, which is worse than the "global optimum". In fact, s' is accepted if s' is better than s , and causes it to be. The probability function P is written as **Equation (4)**.

$$e = \exp\left(-\frac{E(s') - E(s)}{T}\right) \tag{4}$$

If the temperature of T is reduced to zero, the probability of P is also reduced. Obviously, when $e < e'$, the probability function of acceptance is reduced to zero, and when $e' < e$, it tends to be one. Evidently, temperature plays a key role in controlling system changes. As mentioned earlier, the temperature in the simulation gradually decreases. Therefore, the algorithm starts from a very large temperature ($T = \infty$) and it decreases at each stage, according to a pre-determined annealing schedule. Annealing timing is done according to the fact that if the resources used (for example, the amount of calculations) are completed, the processing time will also be completed. Therefore, the algorithm first seeks to respond in a large space of solutions, regardless of the internal energy of the system, and gradually moves to areas with less energy. The area is gradually getting smaller, and this will continue until a "global optimization" is found. To further clarify the issue, the algorithm for doing the work is shown in **Figure 2**.

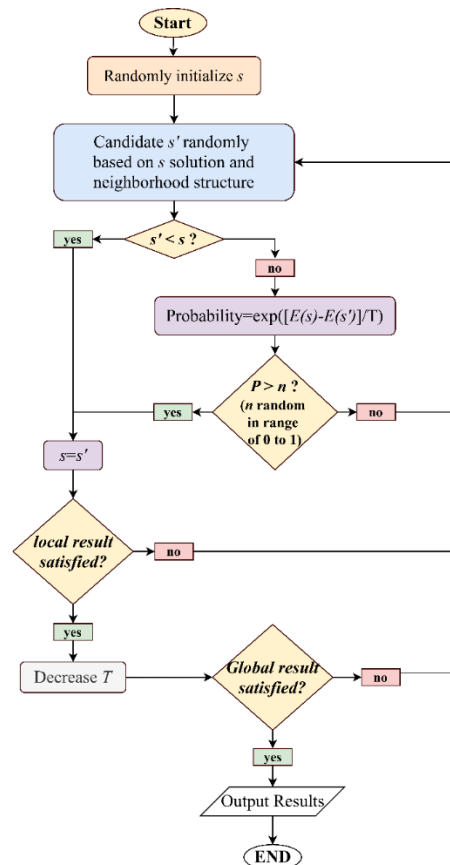


Figure 2: Flowchart of SA algorithm [28]

4. Creating the databank

4.1. Design and analysis of non-linear models

This study is based on 2-D regular frames with a constant height of 3 meters and 5 meters' bays. The columns are pinned connected to the base, and capable of conveying the moment forces along their height. The beams are also pinned connected to the columns. Dead and live uniform loads on beams are 2500 and 1000 kg/m, respectively. Moreover, the yield stress of steels is considered equal to 2400 kg/cm². The number of stories, n_s , is considered to 3-, 6-, 9-, 12-, 15- and 20. Typical configuration of 2-D frames is shown in **Figure 3**. The fundamental period of the frames is calculated by using the relation $T=0.08H^{0.75}$ and considering H as the total height of the frames [29]. Links have been classified

into short, intermediate and long length, which are the same as indicated in previous studies [30–32]. For values less than $1.6M_p/V_p$ (where M_p and V_p are the plastic moment and the plastic shear strengths, respectively), the link behavior is controlled by shear, while for values greater than $2.6M_p/V_p$ it is controlled by flexure. For link lengths between $1.6M_p/V_p$ and $2.6M_p/V_p$, a combination of both shear and flexural yielding occurs [33]. Hence, Models have been developed for these triple link beam length ratio ($\zeta = e/L$), of 0.2, 0.35 and 0.50.

In addition, each model has been expanded with a brace slenderness, λ , in triple level. Slenderness of braces were obtained by using the **Equation (5)** [34].

$$\lambda = \frac{l}{\pi \cdot r} \sqrt{\frac{F_y}{E}} \quad (5)$$

which l is the length of the braces, r is the gyration radius of the bracing section, F_y is the used yielding stress of the steel, and E is the Young's modulus of materials.

The effect of the columns stiffness is given by a coefficient, α , which is calculated as **Equation (6)** [34].

$$\alpha = \frac{n_c \cdot I_c \cdot L_d}{n_d \cdot A_d \cdot h^3 \cdot \cos^2 \theta} \quad (6)$$

where n_c and n_d are the number of columns and the number of braces in a story, respectively. I_c is the second moment of inertia of the columns, h , is the floor height, and θ , is the angle between the brace and the beam.

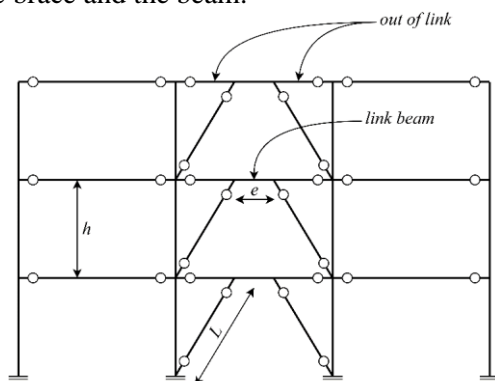


Figure 3: Typical configuration of EBFs

Based on capacity design principles, diagonal braces, columns and beam segments outside of the links are designed to remain essentially elastic [35, 36]. Therefore, these members must have adequate strength to resist forces corresponding to the expected strength of the link, including strain hardening [37]. The braces are designed to have sufficient resistance due to seismic loading equal to forces generated by adjusted link shear strength. The design of the beam outside of the link is similar to the brace. The columns are designed to resist the forces due to the adjusted shear strength of all links above the level of the column.

The EBFs have been designed in accordance with LRFD⁶ method of AISC 360-10 [33] by means of ETABS 2016 [38] software. Thus, a database family of models is generated at $6 (n_s) * 3 (\alpha) * 3 (\lambda) * 3 (\zeta) = 162$ members. In the following, all EBFs has extended with 4 different

⁶ . Load and Resistance Factor Design

rotation angle of link beams values, accordance to the 4 performance levels. The first performance level is related to forming the first plastic hinge in the link beam and the rest of performance levels taken from ASCE41-13 [39], corresponding to the angle of rotation of link beam. Using Equation $\Delta_i = \gamma_i e h / L$, for the quadruple performance levels extracted from ASCE41-13 [39], for the different link beam lengths, the maximum displacement is related to the link beam rotation. Δ_i , γ_i , e , h and L are displacement, link beam rotation, link beam length, story height and brace length respectively. Moreover, extended EBFs are analyzed under 20 pulse-type near-fault earthquakes. OpenSEES [40] software has been employed for the nonlinear time history analyses.

In EBFs, the inelastic response of link beam has been modelled by means of the approach proposed by Bosco *et al.*[41]. The model simulates the effect of the shear force and flexural bending on the inelastic behavior of the link beams with short, intermediate and long length. The link model includes five elements connected in series as shown in **Figure 4**. The middle element (EL0) has the identical length and moment of inertia of the link which allows its flexural elastic response to be considered. There are two zero length elements (EL1 and EL2) in this simulation. (EL1) considers the elastic and inelastic shear response of half a link, while (EL2) considers the inelastic flexural response of the ending part of the link. The nodes EL1 and EL2 are permitted to have independently relative vertical displacements and relative rotations, respectively [41]. Beams, columns, braces and beam segments outside of the links are modelled with the aid of elastic elements to remain essentially elastic. The Rayleigh damping is considered in the analyses. Stiffness and mass coefficients are specified in

order that the first and the third modes of the frame are determined by an equivalent viscous damping factor equal to 0.05.

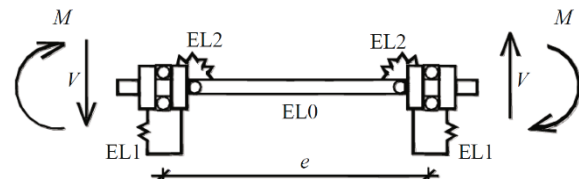


Figure 4: Modelling of the link [41]

4.2. Near-fault records

Near-fault earthquakes are selected based on the classification presented in Baker's study [42]. Characteristics of selected earthquakes are shown in **Table 1**. The final database will be $162 * 4 * 20 = 12960$.

To produce the expected database, 12960-time history analyzes were performed on the basis of an IDA analysis platform, using OpenSEES [40] software. In this regard, records is repeatedly affected by multiplying a Scale-Factor (*SF*) coefficient. Corresponded to the performance levels, the maximum inter-story drift of the frame is compared to the target values of ASCE41-13 [39] in each iteration. The repeat operation continues until the expected values are reached and then stops [43]. The appropriate coefficient for different performance levels is calculated using the Bayesian method. This process is performed for a specific performance level based on the flowchart shown in **Figure 5** for a single earthquake [43].

Researchers have been criticized for scaling, especially when they are above 10 or even 12 [44, 45], cause that the results were within the range of normal earthquakes has led to the elimination of some of the data that claims higher than 12 from the databank. This screening eventually resulted in the use of 9026 net databank from 12960 data. For each data, the maximum roof displacement, $u_{r,max}$, and inter-story drift, IDR_{max} , are calculated.

Table 1: Characteristics of near-fault earthquakes

Record No.	Earthquake Name	Year	Station Name	PGA ^a (g)	Mw ^b	R ^c (km)
1	Imperial Valley-06	1979	EC County Center FF	0.179721	6.53	7.31
2	Imperial Valley-06	1979	El Centro Array #7	0.462394	6.53	0.56
3	Imperial Valley-06	1979	El Centro Array #8	0.467966	6.53	3.86
4	Imperial Valley-06	1979	El Centro Differential Array	0.417229	6.53	5.09
5	Morgan Hill	1984	Coyote Lake Dam (SW Abut)	0.813971	6.19	0.53
6	Loma Prieta	1989	LGPC	0.943935	6.93	3.88
7	Landers	1992	Lucerne	0.704174	7.28	2.19
8	Landers	1992	Yermo Fire Station	0.235782	7.28	23.62
9	Northridge-01	1994	Jensen Filter Plant	0.517814	6.69	5.43
10	Northridge-01	1994	Newhall - Fire Sta	0.723597	6.69	5.92
11	Northridge-01	1994	Rinaldi Receiving Sta	0.869806	6.69	6.50
12	Northridge-01	1994	Sylmar - Converter Sta	0.594294	6.69	5.35
13	Northridge-01	1994	Sylmar - Converter Sta East	0.828472	6.69	5.19
14	Northridge-01	1994	Sylmar - Olive View Med FF	0.732606	6.69	5.30
15	Kobe, Japan	1995	KJMA	0.854262	6.90	0.96
16	Kobe, Japan	1995	Takarazuka	0.645232	6.90	0.27
17	Kocaeli, Turkey	1999	Gebze	0.241333	7.51	10.92
18	Chi-Chi, Taiwan	1999	TCU049	0.286217	7.62	3.78
19	Chi-Chi, Taiwan	1999	TCU053	0.224488	7.62	5.97
20	Chi-Chi, Taiwan	1999	TCU068	0.564477	7.62	0.32

a Peak Ground Acceleration, b Moment Magnitude, c Closest distance from the recording site to the ruptured area e

4.3. Verification

Modeling validation is one of the most important and fundamental steps in any study. This is especially important for analytical studies and research that require a large database. It is clear that if modeling assumptions have errors, the results used in empirical extensions will also be inaccurate. Therefore, for the purpose of validation, a 6-storey structural model has been developed and from the study of Fakhroddini *et al.* [37]. The frame is schematically similar to that shown in **Figure 3**. The uniform story height and bay length are 144 and 360 in, respectively. Considering L , as the length of the beam, three different value, 0.1, 0.3 and 0.5 has taken as a to creating three different link beam values. These link beam lengths, have been classified into short, intermediate and long length, which are the same as indicated in previous studies [30-32]. For values less than $1.6M_p/V_p$ (where M_p and V_p are the plastic moment and the plastic shear strengths, respectively), the link behavior is controlled by shear, while for values greater than $2.6M_p/V_p$ it is controlled by flexure. For link lengths between $1.6M_p/V_p$ and $2.6M_p/V_p$, a combination of both shear and flexural yielding occurs [33]. All frames have three bays with simple beam-to column connections. The uniform dead and live loads of all beams are 0.12 and 0.06 kips/in, respectively, and seismic floor masses of all frames are considered 206 kips. A steel grade of A992 that has a yield strength of 50 ksi is used in the design of all structural

members. Final section sizes of frames are summarized in **Table 2**. The sections mentioned in the Table 2 are W-type for beams and columns. For this purpose, typically the expression 3 (38 14 14) +3 (14 × 30) means that for the three lower and upper floors, sections W14 × 38 and W14 × 30 have been used, respectively. HSS sections have also been used for all braces. The EBFs given in **Table 2** are analyzed to determine their response to the 15 seismic excitations. OpenSEES software has been employed for the nonlinear time history analyses. The inelastic response of link beam has been modelled by means of the approach proposed by Bosco *et al.* (2015) [41]. For each ground motion, the scale factor (SF) of the ground motion which correlate to Life Safe (LS) performance level is determined by incremental dynamic analysis (IDA) based on acceptance criteria of ASCE 41-13 [39]. Finally, the median peak floor displacements have been recorded in compare to the responses from the OpenSEES illustrated in the **Figure 6**. The comparison of the diagrams shown attests to the sufficient accuracy of the modeling phase in this study.

5. Using Artificial Intelligence Models to optimize the behavior factor

Different parameters were selected for this study. Considering the procedure explained in previous section, 12960 data were calculated and used. The selected data were divided into two groups: one group including 6769 data sets used as training data for developing the model, and the rest of 2257 data sets used as test data for verify

the model validation. The training and test data were selected randomly. Proper selection of input and output data can be the first and foremost step in design intelligent and predicting systems. The input data consists of the number

of stories, beam link length to the beam length ratio, braces slenderness, stiffness of columns, fundamental period of structure, roof ductility and behavior factor within the ranges as shown in **Table 3**.

Table 2: Section sizes of the 6St-EBFs in Fakhroddini et al. [37]

Link length $a=e/L$	Side columns	Middle columns	Link beam	Gravity beams	Brace
0.1	3(14×38)+ 3(14×38)	3(14×311)+ 3(14×132)	2(14×53)+3(14×48)	14×109	5(6×1/2)+6×1/4
0.3	3(14×38)+ 3(14×30)	3(14×311) +3(14×132)	4(14×68)+2(14×48)	14×109	3(6×1/2)+3(6×1/4)
0.5	3(14×38)+ 3(14×30)	3(14×426)+ 3(14×176)	2(14×132)+ 4(14×68)	14×109	4(6×1/2)+2(6×1/4)

Table 3: Range of the data used

Parameter	Number of the data		Range of data		Mean data	
	Training data	Test data	Training data	Test data	Training data	Test data
n_s	6769	2257	3-20	3-20	11.7959	11.7939
ζ	6769	2257	0.2-0.5	0.2-0.5	0.34386	0.34381
λ	6769	2257	0.22135- 0.82729	0.22135- 0.82729	0.39832	0.39835
α	6769	2257	0.00362- 0.06122	0.00362- 0.06122	0.01540	0.01540
T_p	6769	2257	0.952-12.845	0.952-12.845	5.06167	5.0688
μ_R	6769	2257	0.35908- 11.9994	0.46211- 11.9818	3.81001	3.76826
q	6769	2257	1-11.956	1-11.979	2.52357	2.52901

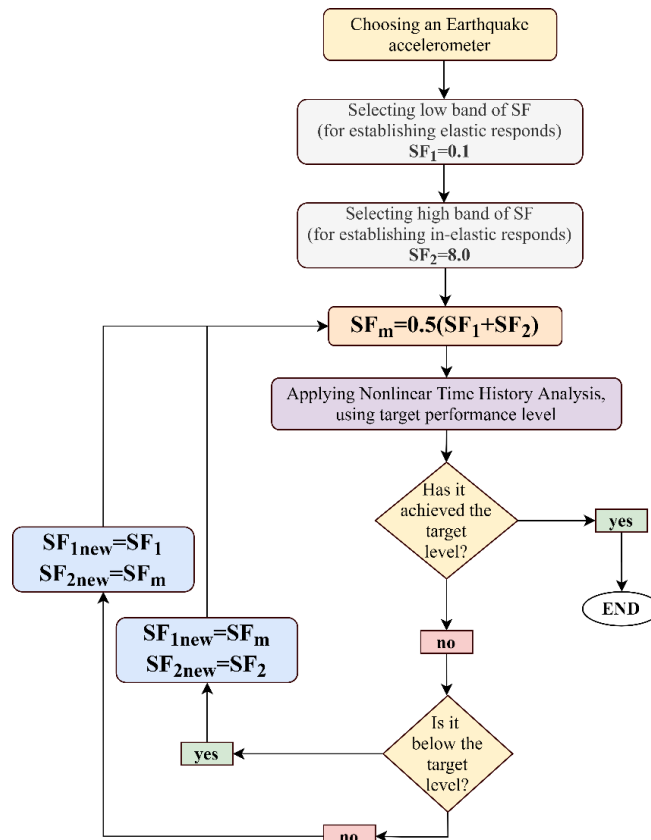


Figure 5: Flowchart of the change in scale factor

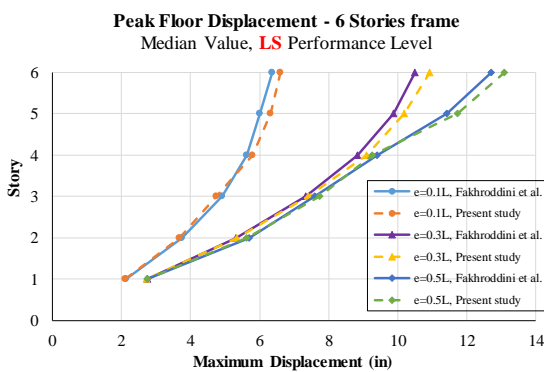


Figure 6: Model validation comparison with the result of Fakhroddini et al. [37]

Several cases were examined by previous researchers [34, 46] to find an appropriate correlation between these parameters for (q) prediction. After several regressive examinations, they found that there is a powerful relationship between the independent parameters, number of stories (n_s), braces slenderness (λ), stiffness of columns (α), fundamental period of structure (T_p) and roof ductility (μ_R) and (q) for central braced steel braced frames under regular earthquakes as shown in Equation (7).

$$q = 1 + p_1 \cdot (\mu_R - 1)^{p_2} \cdot f(n_s, \lambda, \alpha, \frac{T}{T_p}) \tag{7}$$

To account the effect of link beam length, ζ , is considered as an extra parameter to the function. Moreover, due to the properties of

near-fault earthquakes, parameter T/T_p , change to T_p . Therefore, basic platform of the equation will change to the Equation (8). In other words:

$$q = 1 + p_1 \cdot (\mu_R - 1)^{p_2} \cdot f(n_s, \lambda, \alpha, T_p, \zeta) \tag{8}$$

Equation (8) could be rewrite as Equation (9) to be more clear.

ORIGINAL RESEARCH

$$q = 1 + p_1 \cdot (\mu_R - 1)^{p_2} \cdot n_s^{p_3} \cdot \lambda^{p_4} \cdot \alpha^{p_5} \cdot T_p^{p_6} \cdot \xi^{p_7} \tag{9}$$

The roof ductility, μ_R , is obtained by dividing the in-elastic roof displacement, Δ_i , on the yielding displacement, Δ_y , obtained by nonlinear time history and pushover analysis respectively. Accuracy of **Equation (9)** depends on p_1 to p_7 constants. The optimal response for these coefficients is determined by minimizing the difference between predicted and real q . For this purpose, two optimization algorithms including PSO and SA algorithms have been used. These algorithms are among the most powerful artificial intelligence techniques used to solve linear and nonlinear optimization problems. For this purpose, the data were randomly divided into two categories after

loading. One category included 6769 data (approximately 75% of the data) and the other group included 2257 data (approximately 25% of the data), which were used to teach and test algorithms performance, respectively. As a result, 9027 data were used to estimate the coefficients. **Figure 7** shows the real values of q versus the predicted values obtained from the optimization algorithms training data. **Figure 7a** shows these values for the data taught in the PSO algorithm and **Figure 7b** for the data studied under the SA algorithm. In these figures, the horizontal axis represents the number of data used and the vertical axis represents the values of each data.

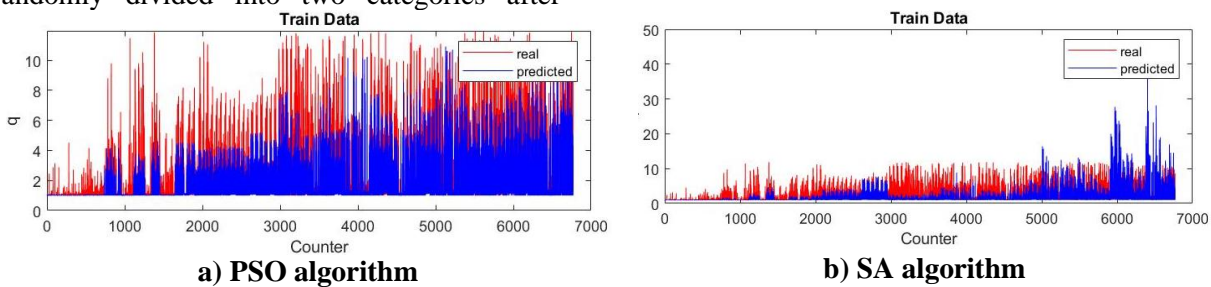


Figure 7: Real and predicted values in **training data** for optimization algorithms

Comparing **Figures (7a)** and **(7b)**, it is found that in the values of the predicted behavior factor obtained from the training data of SA algorithm, exceeding the actual numbers of the data bank have been reported. Therefore, a better match between the predicted and real values is observed in the PSO algorithm. The presence of this error can lead to a lower correlation in the final relationship using this algorithm. In order to evaluate the efficiency and accuracy of the algorithms, different criteria including *Error*, *Mean Error*, *Root Mean Square Error*⁷, percentage of *Mean Absolute Relative Error*⁸

and *Correlation coefficient*⁹ between the values obtained from the real and predicted values were used. **Equations (10)** to **(13)** have been used to calculate each of these criteria. The results of the calculation of these criteria are presented in **Table (7)** for the training data of the two examined algorithms. The correlation between the results of the PSO and SA algorithms and their real values is shown in **Figure 8** for the training data. **Figure 8a** shows these values for the PSO algorithm and **Figure 8b** for the SA algorithm.

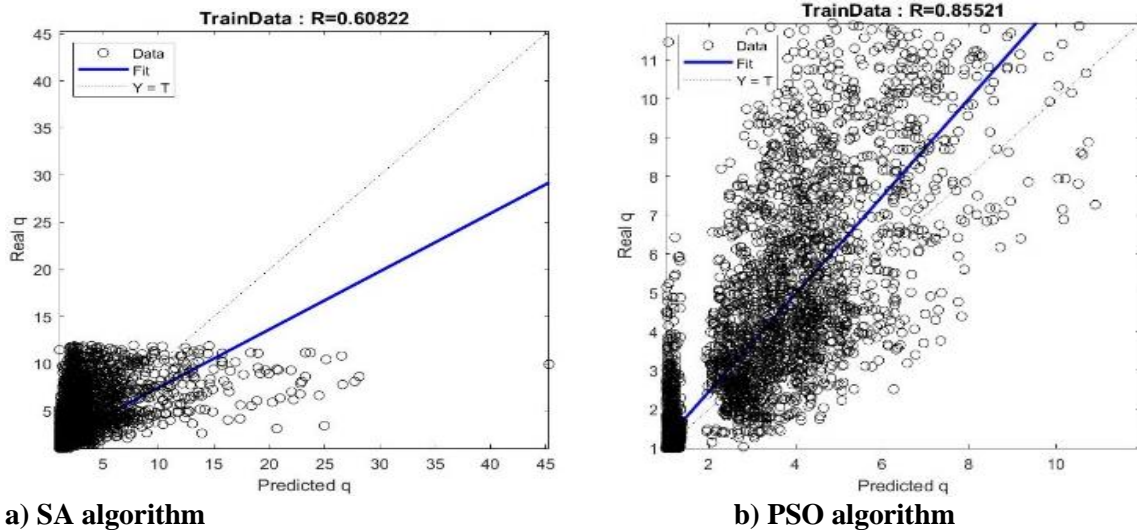
7 . RMSE

8 . MARE

9 . R

$$Error = q_{real} - q_{predicted} \tag{10}$$

$$Mean\ Error = \frac{Error}{N} \tag{11}$$



a) SA algorithm

b) PSO algorithm

Figure 8: Correlation between real and predicted values in training data for optimization algorithms

$$\overline{Error} = \frac{\sum Error}{N} \tag{12}$$

$$RMSE = \sqrt{\frac{\sum Error^2}{N}} \tag{13}$$

Table 4: Error calculation for optimization algorithms based on training data

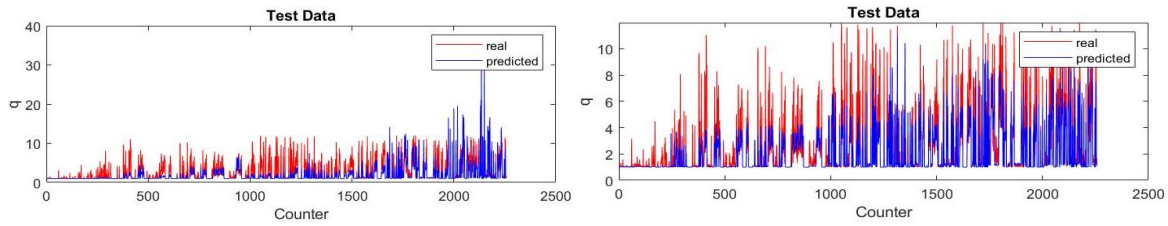
Optimization algorithm	R	Mean Error	Mean Absolute Relative Error	Correlation Coefficient (R)
PSO	0.8552	0.4682	0.1544	0.8552
SA	0.6082	0.5467	0.2168	0.6082

In the above equations, N is the number of categories of data. As can be seen from Table 4, for training data, the Mean Error and RMSE for the model based on PSO were calculated to be 0.46820 and 1.4261, respectively. However, the same values have been reported for the SA algorithm, 0.54672 and 4.9880, which confirms the higher accuracy of PSO in learning the algorithm.

5.1. Correlation validation

To test and validate correlation, 2257 test data were tested. This number was extracted from the total data set of the database randomly and used to test the proposed algorithm. Figure 9 illustrate the predicted and real values of q in the test data. Figure 9a and 9b show the test data values for PSO and SA algorithms, respectively. Also, the correlation between the predicted and real values of q is shown in Figure 10 based on the test data. Figure 10a shows these values for the PSO algorithm and Figure 10b for the SA algorithm.

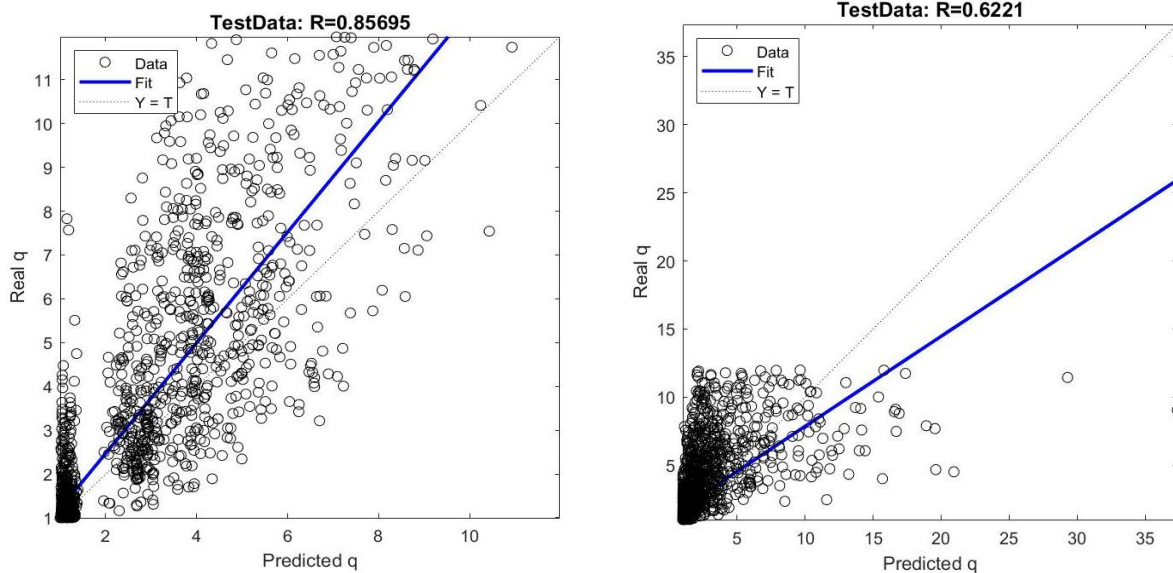
ORIGINAL RESEARCH



a) PSO algorithm

b) SA algorithm

Figure 9: Real and predicted values in test data for optimization algorithms



a) PSO algorithm

b) SA algorithm

Figure 10: Correlation between real and predicted values in test data for optimization algorithms

The criteria for evaluating the efficiency and accuracy of algorithms between the values obtained from the predicted algorithms and the real values used in the algorithm are shown in **Table 5** based on test data.

Table 5: Error calculation for optimization algorithms based on test data

Optimization algorithm	R	Mean Error	Mean Absolute Relative Error	Correlation Coefficient (R)
PSO	1.4487	0.48326	0.1590	0.8569
SA	4.8225	0.58430	0.2115	0.6220

The results of the evaluation of the algorithms examined in **Table 5** show that the Mean Error and RMSE for the model based on PSO were calculated to be 0.48326 and 1.4487,

respectively, while these values were 0.58430 and 4.8225 for the SA algorithm, which confirms the higher accuracy of the correlation established from the PSO algorithm.

Table 6: Coefficients of proposed equation based on PSO algorithm

Constant	$R = 1 + p_1 \cdot (\mu_R - 1)^{p_2} \cdot n_s^{p_3} \cdot \lambda^{p_4} \cdot \alpha^{p_5} \cdot T_p^{p_6} \cdot \xi^{p_7}$
p_1	0.039815
p_2	1.886839
p_3	1.044889
p_4	-0.27037
p_5	-0.11354
p_6	-0.45798
p_7	0.140305

The results of the correlation study created in the studied algorithms, indicate a greater correlation between the model results and the real values obtained from the PSO algorithm. Also, an examination of the error parameters listed in **Table 5** also shows that the error resulting from the model created using the PSO algorithm is less than the SA algorithm. Thus, according to the measurement, the PSO algorithm is recognized as the optimal algorithm and the coefficients p_1 to p_7 mentioned in **Equation (9)**, the result of this algorithm are presented in **Table 6**.

6. Use of the purposed correlation: a simple design example

This section aims to evaluate the ability of correlation in predicting of seismic demand

parameters¹⁰. For this purpose, a 7-storey structure - having a plan of 15 by 15 square meters - 3 bays in each side, each with a length of 5 meters is considered. The story floors are equal to 3.00m and the height of the floor is regularly considered. Thus, the total height of the structure will be $7 \times 3.00 = 21.00\text{m}$. Structural seismic system is eccentrically braced steel frame. The beam to the column connection are pinned. For beam, column and brace section, IPE, HEB and TUBO sections were used respectively, with a yield stress of 3700 kg/cm^2 . Dead and live surface loads are considered 500 and 250 kg/m^2 , respectively. Thus, considering the tributary width of 4m , the dead and live linear load are 1000 and 500 kg/m respectively, on the perimeter frames. Structure designed based on the standard 2800 [29] with PGA of 0.30g and type 2 soil. Based on the seismic live load contribution coefficients in Standard 2800 [29], the $D + 0.2L$ seismic load combination was used to calculate the seismic load of the frame. The structure was designed using the LRFD¹¹ method using ETABS software. For this purpose, the behavior factor, $q = 7$ is selected according to standard 2800 [29]. IPE300, HEB280 and D193.7x6.3 were found for beams, columns and braces respectively. Maximum roof displacement and maximum inter-story drift ratio under reduced spectrum (divided by q) are 0.0633 and 0.00201 m , respectively. Therefore, the maximum in-elastic roof displacement equals:

$$Disp_{max, Roof}^{in.el.} = q \times Disp_{max, Roof}^{el.} = 7 \times 0.0633 = 0.4431\text{m} \quad (14)$$

Also the maximum in-elastic inter-story drift is:

$$IDR_{max}^{in.el.} = q \times IDR_{max}^{el.} = 7 \times 0.00201 = 0.01407 \quad (15)$$

The geometrical values of the studied frame properties are also calculated from the

relationships below. Thus the slenderness coefficient of the braces is equal to:

$$\lambda = \frac{l}{\pi \cdot r} \sqrt{\frac{F_y}{E}} = 0.9603 \quad (16)$$

10 . SDPs

11 . Load and Resistance Design Method

And the effect of the columns stiffness is calculated as follows:

$$\alpha = \frac{n_c \cdot I_c \cdot L_d}{n_d \cdot A_d \cdot h^3 \cdot \cos^2 \theta} = 0.0416 \quad (17)$$

The fundamental period of the structure, equal to $T=0.78s$, according to the 2800 standard [29]. Having the above-mentioned geometrical

parameters, and using the proposed correlation, maximum roof ductility, is calculated $\mu_R=3.112$. Thus the maximum in-elastic roof displacement is:

$$Disp_{max, Roof}^{in.el.} = \mu_R \times Disp_{max, Roof}^{el} = 3.112 \times 0.0633 = 0.1970m \quad (18)$$

On the other hand, corresponding values can be obtained, using nonlinear time history

analysis under near-fault earthquakes and mean value of analysis results:

$$u_{r,max}^{NTHA} = 0.1865m \quad (19)$$

The slight discrepancy between the results of the proposed correlation and the respond of the time history analysis indicates that the proposed correlation is in good agreement.

7. Conclusion

As a result, after studying a considerable number of EBF frames, a nonlinear dynamic analysis of a large database was prepared. Particle Swarm Optimization (PSO) and Simulated Annealing (SA) algorithms are used to extract the correlations. Both algorithms are among the most powerful artificial intelligence techniques in optimization, which have the extraordinary ability to solve complex problems with a large number of variables. As suggested by simple relationships, it is possible to obtain an acceptable estimate of seismic demand parameters without the need for complex analysis. The main emphasis is on introducing the capability of the proposed relationship in adapting them to the framework of design methods based on elastic analysis. The new empirical relation is proposed to predict the behavior factor q for EBF steel frames under the near-fault earthquakes. The proposed correlation is a nonlinear function of number of stories, braces slenderness, stiffness of columns, and fundamental period of structure, link beam to beam length ratio and roof ductility. To evaluate its accuracy, for both aforementioned algorithms, the Mean Squared Error (MSE) and correlation coefficient (R) between predicted values from the proposed correlation and real values in the test data were calculated. The correlation coefficient for PSO and SA

algorithms were 0.8569 and 0.6221 respectively in the test data values. This indicates the higher accuracy of the results of the PSO algorithm. This value was 0.8334 in Razavi *et al.* [9], which was done with the help of genetic algorithm, shows the greater accuracy of the present algorithm. Therefore, the coefficients obtained from the PSO algorithm were introduced as the final result for application in the proposed relation of the behavior factor of purposed EBFs. Finally, a 7-storey steel frame with force factor 7 (2800 standard, Rev 4 for EBF frames) was designed and analyzed using nonlinear time history against acceleration of the present paper to evaluate the robustness of the proposed relationship in estimating the nonlinear displacement of the structure. Then, roof ductility was calculated and the corresponding roof nonlinear maximum displacement was calculated, using the purposed relationship between roof ductility and behavior factor. In the following, the mean value of nonlinear roof displacement obtained from nonlinear time history analysis was compared with the maximum value of nonlinear roof displacement initialized using the proposed relationships in this paper. The results show the capability of the proposed relation in calculating the maximum inelastic roof displacement.

References

- [1] P.R. Santa-Ana, E. Miranda, Strength reduction factors for multi-degree-of-freedom systems, in: Proceedings of the 12th world

- conference on Earthquake Engineering, Auckland, New Zealand, 2000.
- [2] P. Alessandro, Evaluation of overstrength factor of short links in the eccentrically braced frames (EBFs), in: AIP Conference Proceedings, AIP Publishing LLC, 2022, pp. 120005.
- [3] H. Li, W. Zhang, Q. Wei, Seismic demand assessment on K-configuration eccentrically braced frames, in: Structures, Elsevier, 2022, pp. 1225-1238.
- [4] M. Gerami, A. Sivandi-Pour, Performance-based seismic rehabilitation of existing steel eccentric braced buildings in near fault ground motions, The Structural Design of Tall and Special Buildings, 23(12) (2014) 881-896.
- [5] H. Beiraghi, Near-fault ground motion effects on the responses of tall reinforced concrete walls with buckling-restrained brace outriggers, Scientia Iranica, 25(4) (2018) 1987-1999.
- [6] S.A. Razavi, N. Siahpolo, M. Mahdavi Adeli, The Effects of Period and Nonlinearity on Energy Demands of MDOF and E-SDOF Systems under Pulse-Type Near-Fault Earthquake Records, Scientia Iranica, (2020).
- [7] M. Gerami, D. Abdollahzadeh, Local and global effects of forward directivity, Građevinar, 65(11.) (2013) 971-985.
- [8] A. Mashayekhi, M. Gerami, N. Siahpolo, Assessment of higher modes effects on steel moment resisting structures under near-fault earthquakes with forward directivity effect along strike-parallel and strike-normal components, International Journal of Steel Structures, 19(5) (2019) 1543-1559.
- [9] S.A. Razavi, N. Siahpolo, M. Mahdavi Adeli, A New Empirical Correlation for Estimation of EBF Steel Frame Behavior Factor under Near-Fault Earthquakes Using the Genetic Algorithm, Journal of Engineering, 2020 (2020).
- [10] A. Sivandi-Pour, E. Noroozinejad Farsangi, Statistical prediction of probable seismic hazard zonation of Iran using self-organized artificial intelligence model, International Journal of Engineering, 32(4) (2019) 467-473.
- [11] L. Li, Z. Huang, F. Liu, A heuristic particle swarm optimization method for truss structures with discrete variables, Computers & Structures, 87(7-8) (2009) 435-443.
- [12] E. Doğan, M.P. Saka, Optimum design of unbraced steel frames to LRFD–AISC using particle swarm optimization, Advances in Engineering Software, 46(1) (2012) 27-34.
- [13] S. Chatterjee, S. Sarkar, S. Hore, N. Dey, A.S. Ashour, V.E. Balas, Particle swarm optimization trained neural network for structural failure prediction of multistoried RC buildings, Neural Computing and Applications, 28(8) (2017) 2005-2016.
- [14] L. Lamberti, An efficient simulated annealing algorithm for design optimization of truss structures, Computers & Structures, 86(19-20) (2008) 1936-1953.
- [15] N. Ayyash, F. Hejazi, Development of hybrid optimization algorithm for structures furnished with seismic damper devices using the particle swarm optimization method and gravitational search algorithm, Earthquake Engineering and Engineering Vibration, 21(2) (2022) 455-474.
- [16] C. Tort, S. Şahin, O. Hasançebi, Optimum design of steel lattice transmission line towers using simulated annealing and PLS-TOWER, Computers & Structures, 179 (2017) 75-94.
- [17] C. Millan-Paramo, J.E. Abdalla Filho, Modified simulated annealing algorithm for optimal design of steel structures, Revista Internacional de Métodos Numéricos para Cálculo y Diseño en Ingeniería, 35(1) (2019).
- [18] J. Kennedy, R. Eberhart, Particle swarm optimization, in: Proceedings of ICNN'95-International Conference on Neural Networks, IEEE, 1995, pp. 1942-1948.
- [19] Y. Shi, R. Eberhart, A modified particle swarm optimizer, in: 1998 IEEE international conference on evolutionary computation proceedings. IEEE world congress on computational intelligence (Cat. No. 98TH8360), IEEE, 1998, pp. 69-73.
- [20] I.C. Trelea, The particle swarm optimization algorithm: convergence analysis and parameter selection, Information processing letters, 85(6) (2003) 317-325.
- [21] Q. Bai, Analysis of particle swarm optimization algorithm, Computer and information science, 3(1) (2010) 180.
- [22] P. Fourie, A.A. Groenwold, The particle swarm optimization algorithm in size and shape optimization, Structural and Multidisciplinary Optimization, 23(4) (2002) 259-267.
- [23] Y. Ding, W. Zhang, L. Yu, K. Lu, The accuracy and efficiency of GA and PSO optimization schemes on estimating reaction kinetic parameters of biomass pyrolysis, Energy, 176 (2019) 582-588.
- [24] S. Kirkpatrick, C.D. Gelatt Jr, M.P. Vecchi, Optimization by simulated annealing, science, 220(4598) (1983) 671-680.
- [25] K.A. Dowsland, J. Thompson, Simulated annealing, Handbook of natural computing, (2012) 1623-1655.
- [26] B. Suman, P. Kumar, A survey of simulated annealing as a tool for single and multiobjective optimization, Journal of the operational research society, 57(10) (2006) 1143-1160.
- [27] P.J. Van Laarhoven, E.H. Aarts, Simulated annealing, in: Simulated annealing: Theory and applications, Springer, 1987, pp. 7-15.
- [28] D. Delahaye, S. Chaimatanan, M. Mongeau, Simulated annealing: From basics to applications, in: Handbook of metaheuristics, Springer, 2019, pp. 1-35.
- [29] S. No, 2800, Iranian Code of Practice for Seismic Resistant Design of Buildings, 3 (2005).
- [30] M. Bosco, P. Rossi, Seismic behaviour of eccentrically braced frames, Engineering Structures, 31(3) (2009) 664-674.
- [31] A. Kuşyılmaz, C. Topkaya, Design overstrength of steel eccentrically braced frames, International Journal of Steel Structures, 13(3) (2013) 529-545.
- [32] P. Rossi, A. Lombardo, Influence of the link overstrength factor on the seismic behaviour of eccentrically braced frames, Journal of Constructional Steel Research, 63(11) (2007) 1529-1545.

- [33] A. Committee, Specification for structural steel buildings (ANSI/AISC 360-10), American Institute of Steel Construction, Chicago-Illinois, (2010).
- [34] T.L. Karavasilis, N. Bazeos, D.E. Beskos, Estimation of seismic drift and ductility demands in planar regular X-braced steel frames, *Earthquake Engineering & Structural Dynamics*, 36(15) (2007) 2273-2289.
- [35] Kuşy, Displacement amplification factors for steel eccentrically braced frames, *Earthquake Engineering & Structural Dynamics*, 44(2) (2015) 167-184.
- [36] D. Özhendekci, N. Özhendekci, Effects of the frame geometry on the weight and inelastic behaviour of eccentrically braced chevron steel frames, *Journal of Constructional Steel Research*, 64(3) (2008) 326-343.
- [37] A. Fakhraddini, S. Hamed, M.J. Fadaee, Peak displacement patterns for the performance-based seismic design of steel eccentrically braced frames, *Earthquake Engineering and Engineering Vibration*, 18(2) (2019) 379-393.
- [38] V. ETABS, Ultimate, Integrated Software for Structural Analysis & Design, Computers and Structures Inc, (2016).
- [39] R. Pekelnicky, S.D. Engineers, S. Chris Poland, N.D. Engineers, ASCE 41-13: Seismic Evaluation and Retrofit Rehabilitation of Existing Buildings, Proceedings of the SEAOC, (2012).
- [40] F. McKenna, OpenSees: a framework for earthquake engineering simulation, *Computing in Science & Engineering*, 13(4) (2011) 58-66.
- [41] M. Bosco, E.M. Marino, P.P. Rossi, Modelling of steel link beams of short, intermediate or long length, *Engineering structures*, 84 (2015) 406-418.
- [42] J.W. Baker, Quantitative classification of near-fault ground motions using wavelet analysis, *Bulletin of the Seismological Society of America*, 97(5) (2007) 1486-1501.
- [43] A. Tzimas, T. Karavasilis, N. Bazeos, D. Beskos, Extension of the hybrid force/displacement (HFD) seismic design method to 3D steel moment-resisting frame buildings, *Engineering Structures*, 147 (2017) 486-504.
- [44] F. De Luca, I. Iervolino, E. Cosenza, Un-scaled, scaled, adjusted and artificial spectral matching accelerograms: displacement-and energy-based assessment, Proceedings of XIII ANIDIS, "L'ingegneria Sismica in Italia", Bologna, Italy, (2009).
- [45] J. Hancock, The influence of duration and the selection and scaling of accelerograms in engineering design and assessment, Imperial College London (University of London), 2006.
- [46] T.L. Karavasilis, N. Bazeos, D. Beskos, Seismic response of plane steel MRF with setbacks: estimation of inelastic deformation demands, *Journal of Constructional Steel Research*, 64(6) (2008) 644-654.